European Journal of Pharmaceutical Sciences 170 (2022) 106083

Contents lists available at ScienceDirect

European Journal of Pharmaceutical Sciences

journal homepage: www.elsevier.com/locate/ejps

Mechanistic insight into gel-induced aggregation of amorphous curcumin during dissolution process

Jiawei Han [a,1], Luyuan Li [a,1], Zunting Pang [a], Meiling Su [a], Xiaoshuang He [a], Shuai Qian [a], Jianjun Zhang [b], Yuan Gao [a,*], Yuanfeng Wei [a,*]

[a] School of Traditional Chinese Pharmacy, China Pharmaceutical University, Nanjing, 211198, P.R., China
[b] School of Pharmacy, China Pharmaceutical University, Nanjing, 211198, P.R., China

ARTICLE INFO

Keywords:
Curcumin
Amorphous
Dissolution
Gel formation
Gelation elimination

ABSTRACT

Amorphous curcumin (CUR) exhibited a decreased dissolution rate in comparison with the crystalline counterpart due to its gel formation during dissolution. The main purpose of the present study is to explore the mechanism of such gelation phenomenon. It was found that the dissolution of amorphous CUR and gel properties were influenced by the temperature and pH of the media. The formed gels were characterized by TPA, SEM, DSC, XRPD, FTIR and PLM. The results indicated that the gelation process led to the formation of a porous structure in which water molecules infiltrate, and entered into its supercooled liquid state with high viscosity when contacting aqueous media, accompanied by decreased T_g and crystalline transformation. In addition, mixing with hydrophilic excipients (such as hydrophilic silica) accelerated the gel formation of amorphous CUR, while the addition of hydrophobic excipients (such as hydrophobic silica and magnesium stearate) could effectively weaken and even eliminate the gelation, hence significantly improving its dissolution. Furthermore, according to contact angle measurement and fluorescence microscope observation, hydrophilic excipients were found to be able to accelerate water entering into the interior of amorphous CUR, hence facilitating the gelation, while hydrophobic excipients would hinder water infiltration into the powder and thus achieve degelation. In conclusion, it is important to recognize that the gelation potential of some amorphous materials should be considered in developing robust amorphous drug product of high quality and performance.

1. Introduction

Approximately 75% of drug candidates under development show poorly aqueous solubility, which is related to various pharmaceutical performance issues (Franca et al., 2020; Han et al., 2020; Shi et al., 2021). Enhancing in vivo performance of these candidates by solubility/dissolution improvement has become a critical issue for pharmaceutical enterprises to develop effective drugs with rational dosage forms for patients (Qian et al., 2015). To date, various solubilization attempts have been applied for biopharmaceutics classification system (BCS) class II and IV drugs, such as amorphous solid dispersions (Paisana et al., 2021), nanoparticles (Hou et al., 2019), polymeric micelles (Trubitsyn et al., 2019), cyclodextrin inclusion complexes (Tavares et al., 2021), liposomes (Ahmed et al., 2019; Trucillo et al., 2018), self-microemulsion (Pires et al., 2021), etc. Among these strategies, amorphization by disrupting crystal lattice of crystalline drugs is one of the effective techniques to achieve 100% drug load without large volume/mass of dosage caused by the addition of any other excipients (Kasten et al., 2019; Shi et al., 2019; Wang et al., 2019).

Theoretically, amorphous materials with long-range disorder possess higher surface free energy, entropy, and enthalpy, and usually express much higher solubility/dissolution than their crystalline counterparts. Nevertheless, their application is severely restricted by the risk of potential devitrification and loss of above advantages during manufacturing, dissolution, and storage (Wu et al., 2018a). In terms of fast crystallizers, the amorphous solid would initially show supersaturation, but precipitate to the low level of equilibrium solubility of the crystal within minutes (i.e., “spring” effect) (Heng et al., 2019a), like amorphous docetaxel (Wei et al., 2019) and amorphous atorvastatin calcium (Kim et al., 2008). While for slow crystallizers, after achieving supersaturation, slow precipitation with a slow nucleation and crystal growth (i.e., the “parachute” effect) could be observed following the

* Corresponding authors: School of Traditional Chinese Pharmacy, China Pharmaceutical University, Nanjing.
E-mail addresses: newgaoyuan@163.com (Y. Gao), weiyuanfengyuer@yeah.net (Y. Wei).
[1] These authors contributed equally.

https://doi.org/10.1016/j.ejps.2021.106083
Received 28 July 2021; Received in revised form 21 October 2021; Accepted 17 November 2021
Available online 29 December 2021

Ostwald's rule of stages (Fig. S1) (Brouwers et al., 2009; Heng et al., 2019a), such as amorphous ketoconazole (Fung et al., 2018), mebendazole and tadalafil (Wu et al., 2018b). The maintained supersaturation of amorphous drugs allows more free drug in the gastrointestinal tract to be absorbed, and hence increasing oral bioavailability (Huang et al., 2019; Wang et al., 2019). Unlike high solubility/dissolution of amorphous drugs widely reported, some amorphous compounds exhibit abnormal dissolution behaviors accompanied by much lower dissolution in comparison with their crystalline form, which could be attributed to their gelation during dissolution, including amorphous lurasidone hydrochloride (Heng et al., 2019b; Qian et al., 2017), capecitabine (Meulenaar et al., 2013), indomethacin (Heng et al., 2019a), and simvastatin (Ambike et al., 2005).

Gel is a continuous spatial network of molecules connected to each other defined by Flory (Flory and P., 1974), and has a solid-like rheological behavior and is formed by cross-linking of polymer molecules or small molecules via covalent/non-covalent bonding (Heng et al., 2019a; Sahoo et al., 2019). Based on the type of cross-linking, gels are usually divided into two categories: chemical gels cross-linked by covalent bonds owing to irreversible chemical reactions, and physical gels formed by non-covalent bond interactions (such as hydrogen bonding, hydrophobic interactions, π-π stacking and van der Waals force) (Heng et al., 2019b). Actually, gel formation is considered as a balanced result between the tendency of molecular dissolution and aggregation (Estroff and Hamilton, 2004). As the molecules have higher hydration and more aggregation occur simultaneously, this condition leads to gel formation (Baral et al., 2015). So far, macromolecular gels like chitosan (Cok et al., 2020), hyaluronic acid (Kumar et al., 2020; Wang et al., 2020), sodium alginate (Yao et al., 2018), and their formation mechanisms have been extensively explored, while studies on organic small molecular gels were still rarely reported. Now for small molecules, self-assembly through hydrogen bonding, π-π stacking or ionic interaction is one of main mechanisms for gel formation (George and Weiss, 2006; Qian et al., 2017). For example, doxorubicin hydrochloride gelled in sodium chloride solution on account of π-π stacking interaction occurring in its planer aromatic rings (Hayakawa et al., 1990). Crystalline clarithromycin and amorphous lurasidone formed gels in hydrochloric acidic solution attributing to the formation of their hydrochloride salts (Fujiki et al., 2011; Qian et al., 2017).

Curcumin (CUR), a natural polyphenolic and diketone compound extracted from Curcuma longa, has two 2-methoxy phenols attached symmetrically through seven carbon unsaturated diketone linkers, which induces keto-enol tautomerism (Fig. S2a). In solution, there is equilibrium between two tautomers of CUR. Acidic and neutral solutions favor the β-diketo form and the alkaline medium opt for keto-enol tautomer (Matlinska et al., 2018; Sanphui and Bolla, 2018; Sanphui et al., 2011). At present, CUR has gained increasing interest worldwide because of its multiple biological activities (such as antioxidant, antineoplastic, and antimicrobial) (Huang et al., 2019; Wang et al., 2021; Xie and Yao, 2020). However, its therapeutic applications remain limited mainly due to its low aqueous solubility/dissolution with poor oral absorption. In our previous study, amorphous CUR was prepared with the purpose of improving its dissolution (Wang et al., 2019), but when the powders of amorphous CUR came into contact with the dissolution media (pH 1.2 HCl buffer, water, pH 6.8 phosphate buffer), it would quickly aggregate to form a viscous solid-like gel mass, resulting in a low dissolution performance compared to crystalline CUR. At present, the above mechanism could not fully explain such abnormal dissolution performances. Therefore, the present study aims to explore the gelation mechanism of amorphous CUR and attempts to eliminate the gel-induced aggregation (i.e., deaggregation) by mixing a small amount of excipient from a formulation development perspective.

2. Materials and methods

2.1. Materials

Crystalline CUR (> 98%) (Fig. S2a) was acquired from Aladdin Biochemical Technology Co., Ltd. (Shanghai, China). Methanol, Tween-80 and phosphoric acid were supplied from Nanjing Chemical Reagent Co., Ltd. (Nanjing, China). Acetonitrile of chromatographic grade were purchased by Anpel Scientific Instrument Co., Ltd. (Shanghai, China). Hydrophilic silica (Fig. S2b) and hydrophobic silica (Fig. S2c) were obtained from Evonik Degussa Co., Ltd. (Parsippany, USA). Magnesium stearate (Fig. S2d) was provided from Sunhere Pharmaceutical Excipients Co., Ltd. (Anhui, China). Deionized water was prepared by ultrapure water purification system (OLABO, Boke Instruments, Shandong, China).

2.2. Preparation of amorphous CUR and thermogravimetric analysis

Amorphous CUR was prepared by quench cooling method and 185 °C was applied to safely prepare amorphous CUR without thermal degradation. In brief, the temperature of oil bath (DU-20, Yiheng Scientific Instrument, Shanghai, China) was adjusted to 185°C to achieve accurate temperature control (± 1°C). One gram of crystalline CUR was spread and placed in an aluminum foil cup (5.2 cm in diameter). The cup floated on the oil bath until completely melting of CUR (~ 5 min), and then quickly moved onto liquid nitrogen (-196°C) for 2 min. The obtained solid was gently ground with a glass mortar, sieved through 80 meshes, and stored in a desiccator above P_2O_5 and silica gel before analysis. Amorphous CUR, which was investigated by thermogravimetric analyzer (Q500, TA Instruments, New Castle, USA). Crystalline CUR (3 mg) was accurately weighed in an aluminum pan and heated from 30 to 240°C at a rate of 10°C/min under a constant velocity of nitrogen (40 mL/min). On the other hand, the yield of amorphous CUR was determined after the preparation. The sample (approximately 10 mg) was accurately weighed and placed in a volumetric bottle (25 mL) with methanol. The concentration of CUR was analyzed by the HPLC system to further calculate the actual weight in weighed amorphous CUR.

Yield of amorphous CUR (w/w, %) = Actual CUR content determined by HPLC / Weight of amorphous CUR *100%

2.3. Dissolution under non-sink conditions

Dissolution tests of amorphous CUR were conducted in triplicates by a small-volume dissolution apparatus (FADT-1202, Fu Kesi Analysis Instrument Co., Ltd., Shanghai, China) with a constant stirring of 50 rpm in 200 mL phosphate buffer (PBS) with 0.5% Tween-80. Two factors (i.e., temperature and pH value of dissolution medium) were investigated for the effects on dissolution and gel formation of amorphous CUR. Firstly, dissolution tests were conducted in pH 6.8 PBS at different temperatures (25, 37, and 45°C), in order to explore the effect of temperature on gel properties and dissolution behavior. Additional dissolution tests were performed at 37°C in PBS with different pH values (1.2, 4.5, and 6.8). Crystalline CUR and amorphous CUR (100 mg) were added to the dissolution media. At predetermined intervals (0.167, 0.33, 0.5, 0.75, 1, 1.5, 2, 3, 4, 5, 6, and 8 h), 2 mL aliquots were collected into a clean tube, accompanied by the addition of an equal volume of fresh medium immediately. After filtration using a 0.45 μm membrane and dilution with an equal volume of methanol, the CUR concentration was analyzed by the HPLC system (LC-2010A, Shimadzu Co., Ltd., Tokyo, Japan) with an Ultimate C_{18} column (250 mm × 4.6 mm, 5 μm). The mobile phase was composed of a solvent mixture comprising 0.3% phosphoric acid in acetonitrile-water (60:40; v/v) with a flow rate of 1 mL/min at 35 °C. The wavelength for detecting CUR was set at 430 nm (Huang et al., 2019; Wang et al., 2019). All the method data of CUR by HPLC analysis were provided including linearity, accuracy, precision,

and wavelength max spectrum in supplementary material (i.e., Fig. S3, Fig. S4, Table S1 and Table S2).

2.4. Texture profile analysis (TPA)

The formed gels of amorphous CUR were taken out from the medium without drying and evaluated by a Texture Analyzer (CT3, Brookfield, USA) at once. Firstly, the gels were treated using the ZCP020 Manual Cutting Press to prepare the square gel samples (dimensions: length-6.0 mm, width-6.0 mm, height-6.0 mm). Then, the regular gel was placed on a fixed base (TA-BT-KIT) and forming a horizontal surface of contact with the probe. The gels were compressed with a trigger force of 5.0 g under a cylindrical probe (P/0.5R) with diameter of 12.7 mm. The pre-test speed, test speed and post-test speed were set at 1.0 mm/s, 5.0 mm/s and 5.0 mm/s, respectively. Texture parameters measured including adhesiveness, springiness and cohesiveness were collected to analyze the gel properties.

2.5. Scanning electron microscopy (SEM)

The surface morphology of amorphous CUR before and after dissolution under various conditions was examined by a SEM system (SU500, Hitachi Ltd., Tokyo, Japan). The instrument was operated with probe current 45 nA, accelerating voltage 3 kV and counting time 60 s, respectively. The tested samples were fixed using double-sided adhesive tape and coated with a thin layer of gold before observation.

2.6. Differential scanning calorimetry (DSC)

The collected samples after dissolution of amorphous CUR were performed on a thermal analyzer system (DSC 3500, NETZSCH Co., Selb, Germany) for thermal analysis. The formed aggregate of amorphous CUR was taken out from the medium and analyzed using DSC immediately, or dried with filter paper and vacuum for 48 h prior to DSC analysis to assess the impact of water on the glass transition temperature (T_g) of the gelled mass. Then, the aggregate was gently crushed and dispersed into small particles. The obtained sample (5 mg) was heated to 240 °C in a sealed aluminum pan at 10 °C/min under nitrogen flow with a rate of 50 mL/min. NETZSCH Proteus software (version 6.1.0) was used to analyze the data.

2.7. Thermogravimetric Analysis (TGA)

The collected gels from dissolution of amorphous CUR at different temperatures or pH were heated at 10°C/min under nitrogen purge (50 mL/min) from room temperature to 240°C (TGA Q50, TA Instruments, DE, USA). The water contents of gels were determined based on the % weight loss during heating.

2.8. X-ray powder diffraction (XRPD)

The gels formed after dissolution of amorphous CUR at different temperatures or pH were removed water with filter paper immediately and dried by vacuum for 48 h. XRPD diffractograms of amorphous CUR and the formed gels were acquired using X-ray diffractometer (XPert Powder, Malvern Co., England) with Cu-Kα radiation of 1.5406 Å. The diffractometer was operated with a constant voltage (40 kV) and a steady tube current (100 mA). The sample was scanned at a step size of 0.02° in the scanned range of 5 ~ 40° (2θ).

2.9. Fourier transform infrared spectroscopy (FTIR)

FTIR spectra of collected samples before and after dissolution of amorphous CUR were recorded on a FTIR spectroscopy (IRAffinity-1S, Shimadzu Co., Ltd., Tokyo, Japan) equipped with LabSolutions IR software. Each sample was mixed with KBr for tablet compaction, and the tablet was scanned 45 times at a resolution of 4 cm^{-1} in wavelength coverage of 400 ~ 4000 cm^{-1}.

2.10. Polarizing light microscopy (PLM)

PLM (Eclipse Ci-POL, Nikon Ltd., Tokyo, Japan) was applied to distinguish the emergence of crystals from amorphous CUR under various dissolution conditions. In brief, a small amount of sample was placed on a glass slide, and then fixed with liquid paraffin to disperse it thoroughly. The surface morphology and birefringence phenomenon were observed and recorded by PLM under 10 × 10 times magnification.

2.11. Effect of excipients on the gelation and dissolution of amorphous CUR

From a formulation development perspective, two common glidants, hydrophilic silica, hydrophobic silica and one lubricant, magnesium stearate, were added and evenly mixed with amorphous CUR at weight ratios of 2%, 4% and 6%, with the purpose to investigate their effect on the aggregation of amorphous CUR and its dissolution performance. The dissolution tests were carried out in pH 6.8 PBS at 37°C. Other test conditions were the same as above (section 2.3). Student's t-test was used for statistical analysis of dissolution difference. Differences were statistically significant when $p < 0.05$.

The wettability of amorphous CUR after mixing with hydrophilic silica, hydrophobic silica and magnesium stearate was monitored by contact angle measurement. After ultrapure water was dropped on the tablet surface, and then a contact angle apparatus (OCA15EC, Data-physics Ltd., Germany) was used to determine the contact angle. Furthermore, fluorescence microscopy (F-4500X, Hitachi Ltd., Tokyo, Japan) was used to assist the observation of the above three excipients on the effect of water into the amorphous powder. A small amount of powders (amorphous CUR, and amorphous CUR mixing with 4% hydrophilic silica, hydrophobic silica or magnesium stearate) were placed on a glass slide and covered with a cover glass. Then, a drop of water seeped through the edge of the cover glass.

To further explore the influence of hydrophilic and hydrophobic excipients on aggregation (initial gelation phase) time of amorphous CUR, other six hydrophilic excipients (glucose, lactose, maltose, sucrose, mannitol and sodium chloride) and six hydrophobic excipients (calcium carbonate, calcium hydrophosphate, monocalcium phosphate, calcium citrate, magnesium trisilicate and saccharin) were added into amorphous CUR and uniformly mixed at a weight ratio of 4%. The aggregation experiments were performed in pH 6.8 PBS at 37°C. The aggregation time was determined from the powder spread and put into the medium to the time of the powder aggregation with complete wetting.

3. Results and discussion

3.1. Preparation of amorphous CUR

The preparation of amorphous CUR was studied by thermogravimetric analysis (TGA) to investigate whether crystalline CUR underwent thermal degradation during the preparation process. As depicted in Fig. S5, no weight loss occurred in crystalline CUR and a steep descent appeared in the TGA profile above 198.1°C, which was basically consistent with the previous report (194°C) by Chen et al (Chen et al., 2014). The thermal degradation range of CUR was much higher than its melting point as described in section 3.4 (T_m = 182.6°C) as well as the selected melting temperature (185°C). This result suggested that amorphous CUR could be safely prepared by quench cooling. At last, amorphous CUR was successfully prepared with a high yield of 97.03 ± 0.57%.

3.2. Dissolution behaviors and gel properties under various conditions

Visually, the powders of crystalline CUR and amorphous CUR were yellow and orange red, respectively (Fig. 1a & 1b), which was consistent with the previous report (Sanphui and Bolla, 2018). Crystalline CUR was easily dispersed and suspended in pH 6.8 PBS at the different temperatures (Fig. 1c and Fig. S6). However, when amorphous CUR contacted with the dissolution medium, it would float on the surface of the medium and gradually gather to form a soft and viscous mass (Fig. 1d-f and Fig. S6). After dissolution, the irregular mass appeared as a dark brown aggregate, and was collected for further analysis (Fig. 1e). If the mass was pressed or stretched by hand, it displayed strong resistance to tensile deformation (Fig. 1f), which was consistent with the characteristics of gel, including viscosity of liquids and elasticity of ideal solids. Gelation phenomena of amorphous CUR were also observed during dissolution at 25°C and 45°C. Similarly, amorphous powder floated on the surface of the three different pH media (Fig. S7). As the stirring progressed, the powder gradually gathered into groups, forming sticky masses with viscoelastic properties. On the other hand, the color changes of CUR were observed during preparation and gel formation of amorphous CUR (Fig. S8). At first, crystalline CUR was yellow, but after preparation into amorphous CUR, it turned dark brown and became orange-red after further grinding, which was consistent with the previous report (Sanphui and Bolla, 2018). Upon contact with the dissolution medium, it slowly aggregated and turned dark brown (i.e., the color of the formed gel). The removed gel was dried and ground and then turned orange-red again. The color change might be due to keto-enol tautomerism of CUR as previously reported (Kaur et al., 2018; Kim et al., 2021). In addition, the purity of the formed gels after dissolution was analyzed by the HPLC system and shown in Table S3.

The dissolution curves of crystalline CUR and amorphous CUR in pH 6.8 PBS at 25°C, 37°C and 45°C are shown in Fig. 2A. Consistent with Noyes-Whitney dissolution model, since increasing medium temperature enhanced the diffusivity coefficient and solubility, the dissolution of crystalline CUR gradually improved until reaching the corresponding saturated concentration. Theoretically, amorphous drugs with lattice destruction and long-range disorder tend to exhibit higher solubility/dissolution extent compared with their crystalline counterparts due to larger Gibbs free energy. Nevertheless, amorphous CUR exhibited a lower dissolution than crystalline CUR before 8 h at 25 °C. For dissolution at 37 °C, amorphous CUR exhibited a lower amount dissolved than that of its crystalline counterpart before 6 h, but followed by a slightly higher amount dissolved afterwards. Furthermore, the dissolution rate of amorphous CUR at 45 °C was significantly lower than that of crystalline CUR. At 8h, the dissolution concentration of amorphous CUR in pH 6.8 PBS at 45°C only reached 68% that of the crystalline form on the average. In summary, amorphous CUR showed the lower dissolution rate than crystalline CUR at all tested temperature and pH conditions.

Based on the Noyes-Whitney dissolution model (the following equation) (Forster and Lebo, 2021; Wimalasiri et al., 2021), the dissolution rate of the drug (dC/dt) is associated with D, S, h and C_s. Where D is the diffusivity coefficient, h is the thickness of the diffusion layer, S is the surface area of the sample, C is the concentration of dissolved drug and C_s is the drug solubility in the dissolution medium.

$$\frac{dC}{dt} = \frac{DS}{h}(C_s - C)$$

For crystalline CUR, increased temperature improved the diffusivity coefficient and solubility of crystalline CUR, promoting its dissolution (Table S4). While for amorphous CUR, increased temperature not only affected its diffusivity coefficient and solubility, but also the gelation of amorphous CUR and hence its surface area. Therefore, the medium temperature and degree of gelation were competitive for the dissolution of amorphous CUR. Increasing temperature from 25 °C to 37 °C effectively enhanced the diffusivity coefficient and solubility of CUR, facilitating the dissolution of amorphous CUR despite the gel formation. While as the medium temperature rose from 37 °C to 45 °C, more important gelation of amorphous CUR caused a more compact mass with the significant decrease of surface area, resulting in the lowest dissolution rate at 45 °C. This higher gelation at high temperature is illustrated

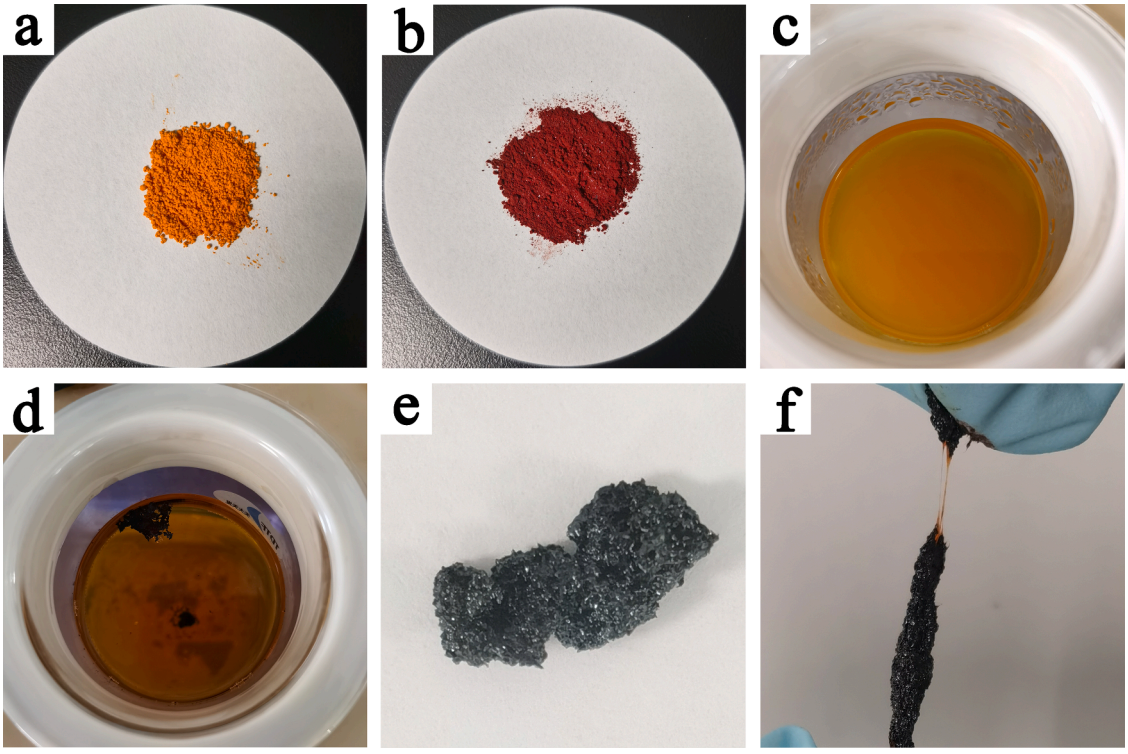

Fig. 1. Photographs of (a) crystalline CUR powder, (b) amorphous CUR powder, and (c) crystalline CUR, (d) amorphous CUR, (e) the formed gel after dissolution in pH 6.8 PBS at 37°C as well as (f) the stretched gel.

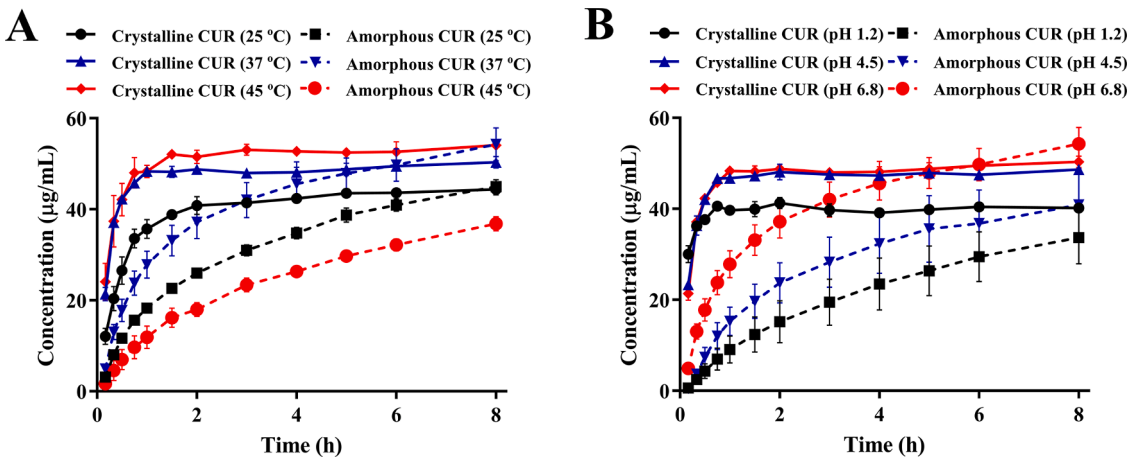

Fig. 2. (A) Dissolution profiles of crystalline CUR and amorphous CUR in pH 6.8 PBS at 25, 37, and 45°C (n = 3). (B) Dissolution profiles of crystalline CUR and amorphous CUR in pH 1.2, 4.5, and 6.8 PBS at 37°C (n = 3).

by the higher cohesiveness of the gel obtained by texture analysis.

The dissolution profiles of crystalline CUR and amorphous CUR in pH 1.2, 4.5, and 6.8 PBS at 37°C are depicted in Fig. 2B. As CUR is a polyphenolic compound, the existence of phenolic hydroxyl groups in its molecular structure shows a weak acidity and a certain pH dependence (Fig. S9) (Piovesan et al., 2020). For crystalline CUR, its dissolution in pH 6.8 medium was slightly higher than that in pH 4.5 medium, while it showed the lowest dissolution rate in pH 1.2 medium. However, the dissolution of amorphous CUR in pH 6.8 medium was lower than that of crystalline CUR in the first 6 h, while in the pH 4.5 and pH 1.2 media, amorphous CUR exhibited significantly lower dissolution rate in comparison with its crystalline form throughout the whole dissolution tests. Based on the Noyes-Whitney equation, the dissolution was mainly affected by the C_s differences of CUR in three pH media. Furthermore, the pH dependence was further amplified for amorphous CUR due to gel formation, which showed a more obvious pH dependence with the order of pH 1.2, 4.5 and 6.8.

Evaluated texture parameters of the formed gels by texture analyzer, including adhesiveness, springiness and cohesiveness, are depicted in Fig. 3 and Fig. S10. It was found that the adhesiveness of the formed gels increased significantly with increasing temperature of the medium. Adhesiveness represents the surface characteristics affected by adhesive and cohesive forces (Huang et al., 2007). When the medium temperature went from 25°C to 45°C, the adhesiveness of formed gels significantly increased by 17.3-fold, which resulted in the slow dissolution of amorphous CUR. Springiness, also called elasticity, is also the measure about how fast structure regains its original shape if the stress is removed. Cohesiveness, as another parameter of the coefficient of difficulty for breaking the structure inside of the gel, is about interaction being stronger for the like entities which makes it difficult to form interaction with another chemical moiety (in this case water) (Heng et al., 2019a; Heng et al., 2019b). When the medium temperature went from 25°C to 45°C, the springiness and cohesiveness of formed gels improved dramatically from 0.17 to 0.99 and 0.24 to 0.89, respectively, indicating that the internal structure of gels became more compact and was hard to break. Under different pH conditions, the texture parameters of formed gels did not show significant difference.

3.3. SEM

The SEM analysis was conducted to detect morphology of the formed gels from amorphous CUR under different dissolution conditions. As seen from Fig. 4, the original crystalline CUR displayed a rodlike or columnar-like (Fig. 4a), while its amorphous form appeared an irregular block shape (Fig. 4b). The collected sample after dissolution of crystalline CUR shared similar morphology with original one (Fig. 4c). However, amorphous CUR agglomerated into big irregular masses. When the dissolution temperature went from 25 °C to 45 °C, the microstructure of agglomerate became visually more compact (Fig. 4d-f), which might be caused by the increase of gel adhesiveness. Besides, there was no significant difference in the morphology of the formed gels in three different pH media (Fig. 4g-i). In order to further monitor the aggregation process, the collected samples at different time points were inspected under SEM (Fig. 5). At the initial 30 min, the collected samples exhibited as agglomerates with porous 3-D structure (Fig. 5a & 5b). Afterwards, the surface particles on the agglomerate linked together accompanied by the disappearance of internal pores gradually (Fig. 5c & 5d).

3.4. DSC and TGA

DSC and TGA studies were carried out to characterize and analyze

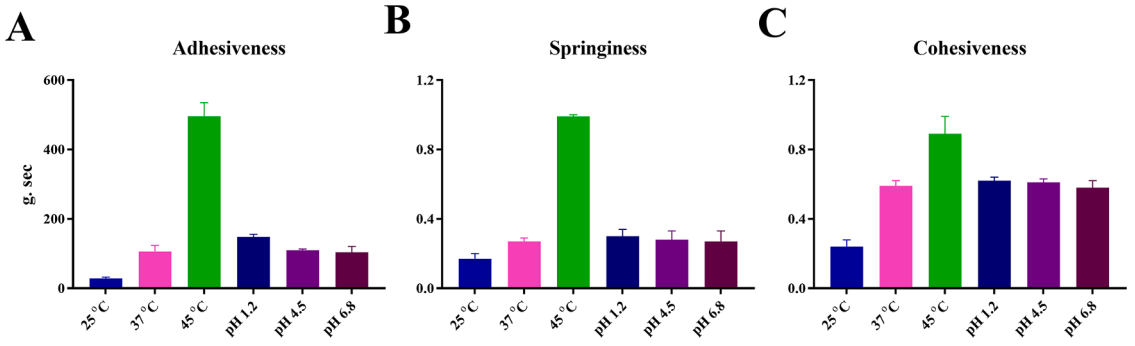

Fig. 3. Texture parameters of the formed gels from amorphous CUR after dissolution under various conditions (n = 3).

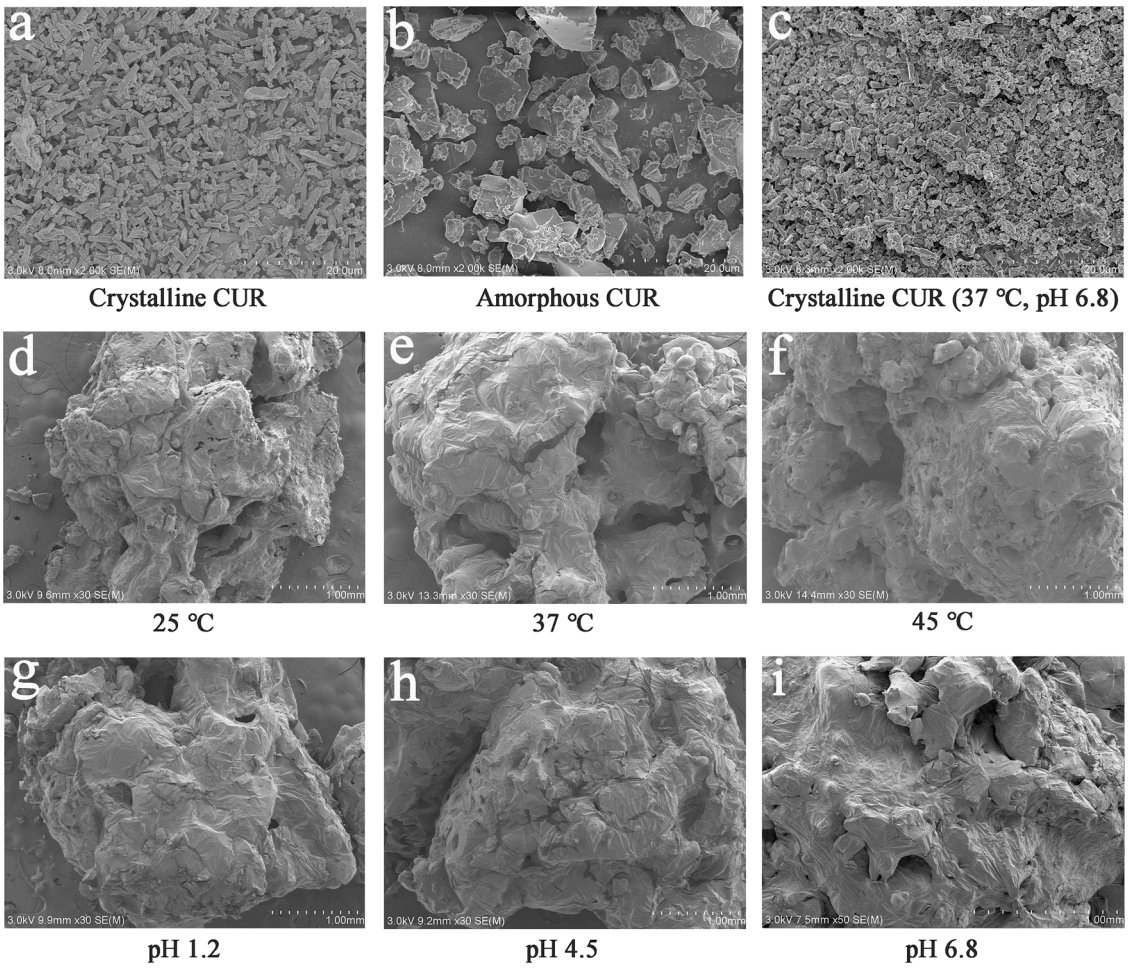

Fig. 4. SEM images of (a) crystalline CUR, (b) amorphous CUR, (c) crystalline CUR after dissolution in pH 6.8 PBS at 37°C, and the gels formed from amorphous CUR in pH 6.8 PBS at (d) 25, (e) 37 and (f) 45°C; or in (g) pH 1.2, (h) 4.5, and (i) 6.8 PBS at 37°C.

the thermal properties of crystalline CUR, amorphous CUR and the formed gels under various conditions. As shown in Fig. 6, crystalline CUR exhibited a representative curve of melting endotherm at 182.6 °C, which was the endothermic melting peak of crystalline form (Fig. 6a and Fig. S11A). Amorphous CUR showed a T_g of 74.5 °C without the melting peak (Fig. 6b and Fig. S11B), which was different from T_g (about 60 °C) previously reported by Sanphui et al (Sanphui and Bolla, 2018; Sanphui et al., 2011). Both amorphous CUR materials were prepared by quench cooling method. In the previously reported study, CUR melt was cooled down to room temperature (25 °C). However, liquid nitrogen (-196 °C) was used for cooling in the current study. The differences in preparation parameters (including cooling rate) affected the degree of disorder in the solid material and hence made a difference in T_g values (such as amorphous indomethacin and amorphous d-mannitol) (Karmwar et al., 2012; Zhu et al., 2015). The formed gels by vacuum drying showed no obvious dehydration peaks by TGA analysis (Fig. S12), indicating that no water was present in the vacuum-dried gels to ensure no effect on the T_g. The dried gels performed similar thermal behaviors with a reduced T_g and an endothermic peak around 182 °C (Fig. 6c-h), indicating the recrystallization of amorphous CUR during dissolution. Moreover, the area of endothermic peak (CUR crystallization enthalpy) enlarged with increasing temperature from 25 °C to 45 °C, which was because the increased temperature caused the CUR molecules to move faster and promoted the nucleation and crystal growth, resulting in more crystalline transformation (Fig. 6c-e). However, the crystallization enthalpy of gels at around 182 °C was relatively low in comparison to crystalline CUR, suggesting the low degree of crystalline transformation.

Furthermore, overlay of modulated DSC/TGA of samples removed immediately after dissolution are depicted in Fig. 7, the formed gels under 25, 37 and 45°C conditions contained the water contents of 5.42%, 8.21% and 11.05% by TGA analysis (Fig. 7A-C), respectively, which was consistent with the trend of non-reversing heat flow in modulated DSC curves. Meanwhile, the higher water content resulted in higher viscoelasticity of the gel (Fig. 3). Besides, the water contents of the formed gels removed from pH 1.2, 4.5 and 6.8 media were 13.33%, 10.49% and 9.68%, respectively (Fig. 7D-F). The weight loss in TGA curves were well correlated with non-reversing heat flow of modulated DSC curves. Large endothermic behavior started from room temperature was caused by loss of surface water. As seen from the reversing heat flow curves, the formed gels showed significantly reduced T_gs (17-25 °C). As is well known, the plasticizing effect of water could cause a decrease in the T_g of amorphous drug, which would lead to the transformation of amorphous glassy state into its supercooled liquid (Edueng et al., 2017). Based on SEM, TGA and DSC analysis, such gelation process in a water environment was put forward and schematically described in Fig. S13 & 8. The dispersed amorphous powders kinetically adhere together to form agglomerated particles once contacting with the aqueous medium, gradually forming the gel mass (Fig. S13). In aqueous environment, the aggregate initially formed a porous surface. Due to water plasticization, the amorphous powder changed from its glassy state to supercooled liquid state with high viscoelasticity as dissolution progressed. As water molecules entered through the surface pores, more drug molecules came into contact with the water and gradually adhered to each other, forming a tight network inside. Meanwhile, more water molecules

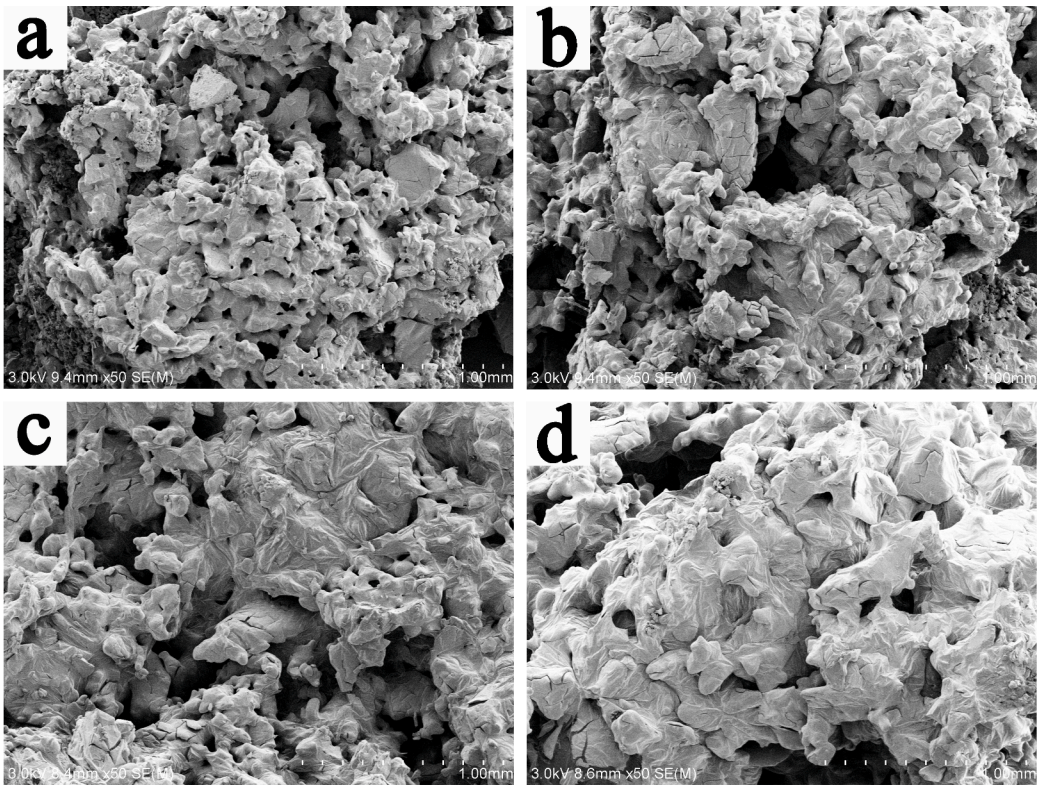

Fig. 5. SEM images of samples collected at 10, 30, 60, and 120 min during dissolution of amorphous CUR in pH 6.8 PBS at 37°C.

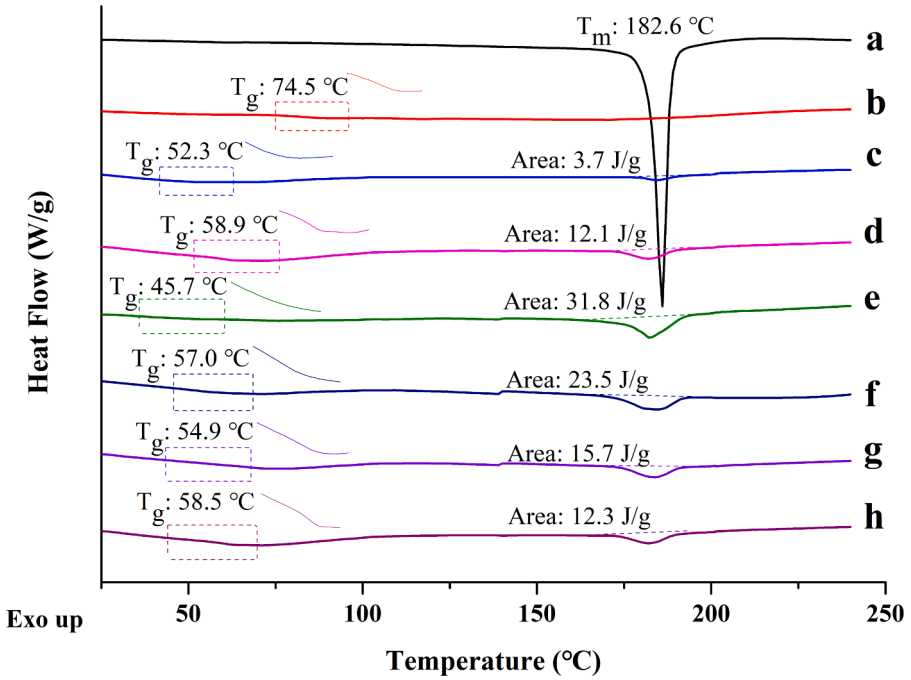

Fig. 6. DSC thermograms of (a) crystalline CUR, (b) amorphous CUR, and the dried gels formed from amorphous CUR in pH 6.8 PBS at (c) 25, (d) 37 and (e) 45°C; or in (f) pH 1.2, (g) 4.5, and (h) 6.8 PBS at 37°C.

entered the interior and were trapped in the network structure, causing the gel to expand in size (Fig. 8).

3.5. XRPD

XRPD was applied to determine the change of diffraction peaks of amorphous CUR before and after dissolution under various conditions. As observed in Fig. 9A, crystalline CUR appeared the intense diffraction peaks at 8.91°, 12.26°, 13.82°, 14.52°, 17.16°, 18.18°, 19.43°, 21.15°, 23.30°, 23.69°, 24.71°, 25.63°, 26.65° and 27.41° for 2θ scan (Fig. 9Aa). In comparison to the reported XRPD patterns, the diffraction peaks located at same positions, indicating the studied CUR was crystalline

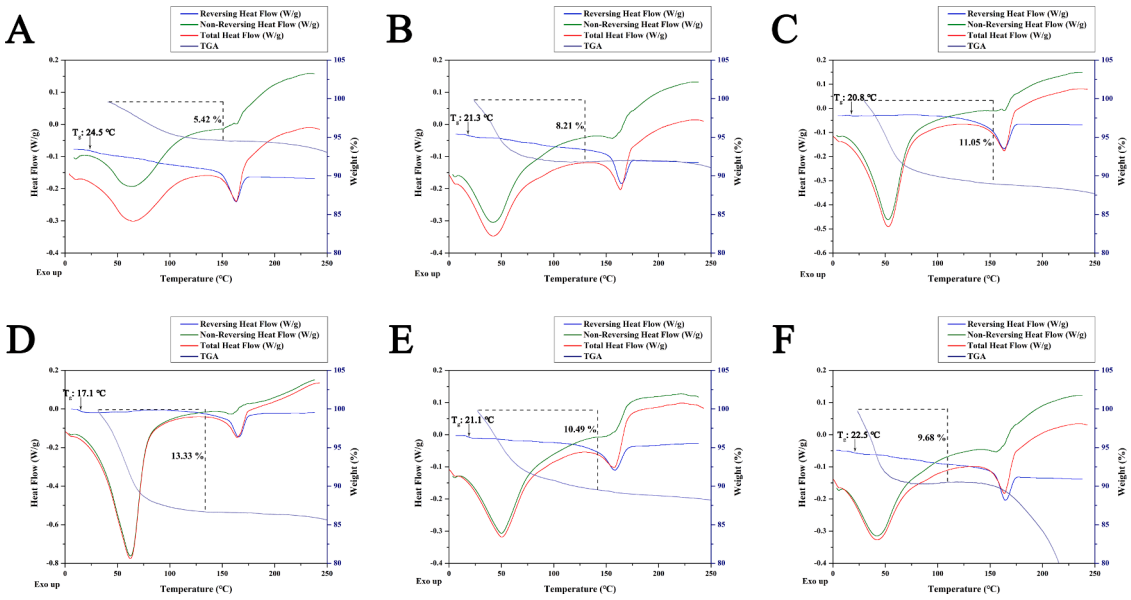

Fig. 7. Overlay of modulated DSC/TGA of the gels removed from pH 6.8 PBS at (A) 25, (B) 37 and (C) 45°C; or (D) pH 1.2, (E) 4.5, and (F) 6.8 PBS at 37°C.

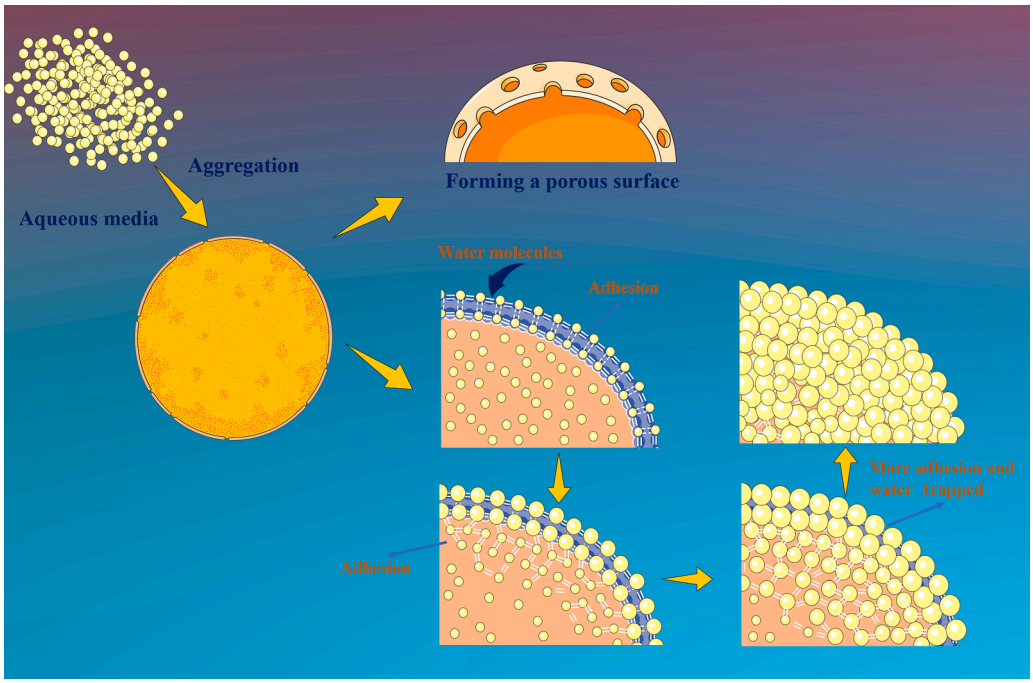

Fig. 8. Proposed schematic diagram of gel formation of amorphous CUR.

form I (Matlinska et al., 2018; Sanphui and Bolla, 2018; Sanphui et al., 2011). For amorphous CUR, the XRPD diffractogram exhibited a typical halo with absence of crystalline diffraction peaks, suggesting the complete amorphization (Fig. 9Ab). As the medium temperature increased, the diffraction peak intensity of the formed gels strengthened relatively, indicating that more amorphous CUR transformation to its crystalline state occurred during gelation (Fig. 9Ac-e). Thermodynamically, increasing temperatures accelerated the motion of CUR molecules, causing more molecules to nucleate and grow. In addition, in gels formed under various pH conditions, amorphous CUR also showed weak characteristic diffraction peaks from crystalline CUR (Fig. 9Af-h), suggesting less recrystallization of amorphous CUR.

3.6. FTIR

As shown in Fig. 9B, crystalline CUR showed distinct characteristic peaks at 3506 cm^{-1}, 1628 cm^{-1} and 1603 cm^{-1} in its FTIR spectrum, which was attributed to the OH group, C=O group and benzene ring vibration, respectively (Fig. 9Ba). As for amorphous CUR, the stretching vibration of the OH group (3506 cm^{-1}) disappeared, and the characteristic peaks shifts (C=O group from 1628 cm^{-1} to 1626 cm^{-1} and benzene ring vibration from 1603 cm^{-1} to 1587 cm^{-1}) and peak broadening with strength reduction were observed after amorphization (Fig. 9Bb), which might be due to the destruction of ordered crystal lattice and the reconfiguration of CUR molecules (Heng et al., 2019b). Under different conditions, the formed gels exhibited similar FTIR spectra to amorphous CUR (Fig. 9Bc-h), suggesting most majority of

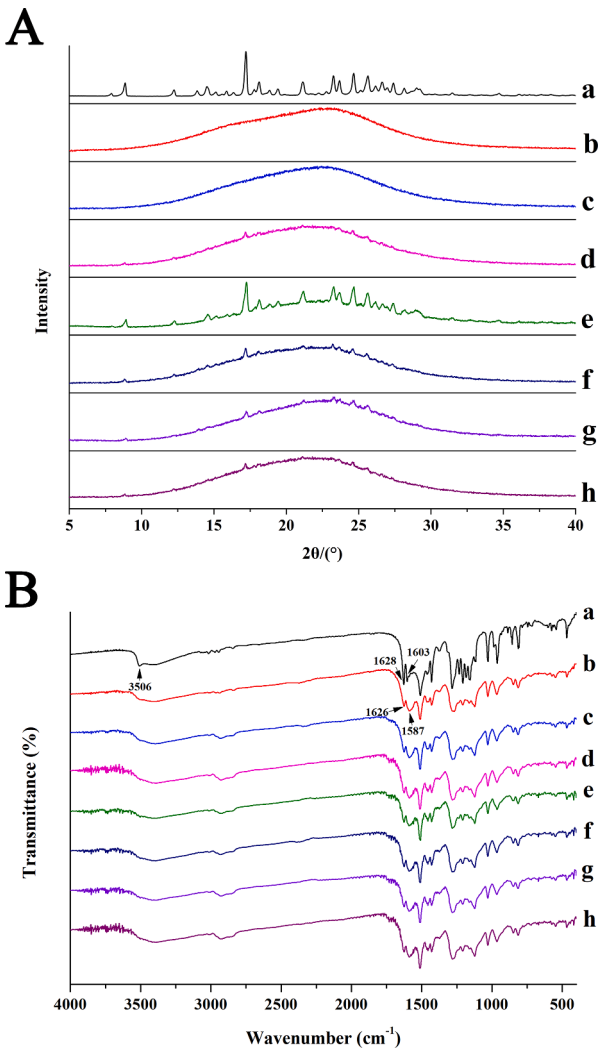

Fig. 9. (A) XRPD diffractograms and (B) FTIR spectra of (a) crystalline CUR, (b) amorphous CUR, and the gels formed from amorphous CUR in pH 6.8 PBS at (c) 25, (d) 37 and (e) 45°C; or in (f) pH 1.2, (g) 4.5, and (h) 6.8 PBS at 37°C.

residual substances still maintained in amorphous state, which was consistent with XRPD results. In addition, weak absorption peaks at around 3000-2750 cm^{-1} in the formed gels might be attributed to C-H vibrations on the benzene ring as previously reported in the literatures (Bhasker-Ranganath et al., 2021; Kim et al., 2013; Ray et al., 2016; Satapute and Jogaiah, 2021).

3.7. PLM

PLM images of amorphous CUR collected at different time points during dissolution are shown in Fig. 10. Crystalline CUR showed obvious birefringence (Fig. 10a), while amorphous CUR prepared by quenching cooling had no birefringence under PLM, suggesting a complete amorphousness (Fig. 10b). The powders of amorphous CUR gradually agglomerated over time at three different temperatures (Fig. 10c-e). The higher the temperature, the more serious the powder aggregation, indicating more significant gelation. Among them, no crystal birefringence occurred within 60 min at 25°C, while birefringence was observed in 10 min at 37°C and in 5 min at 45°C, respectively. The results showed that crystalline transformation occurred during gelation of amorphous CUR, and the higher the temperature was, the faster crystalline transformation would be. In addition, amorphous CUR exhibited similar gelation processes with the appearance of crystal birefringence at 10 min in pH 1.2, 4.5 and 6.8 PBS (Fig. S14). Meanwhile, combined with DSC and XRPD analysis (Fig. 6 and Fig. 9A), the endothermic event (crystallization enthalpy) and diffraction peak intensities of gels were very low relative to crystalline CUR, suggesting that the degree of crystalline transformation was low in the whole dissolution process. Therefore, the decrease in dissolution of amorphous CUR was due to gel-mediated aggregation rather than rapid crystallization.

3.8. Effect of excipients on dissolution and gelation of amorphous CUR

Amorphous CUR in absence and addition of hydrophilic silica, hydrophobic silica and magnesium stearate (2%, 4%, and 6%, w/w) showed different dissolution behaviors (Fig. 11). In comparison with amorphous CUR, dissolution of CUR decreased after addition of hydrophilic silica (Fig. 11A). Nevertheless, the dissolution of amorphous CUR was significantly improved after uniformly mixing with hydrophobic silica and magnesium stearate (Fig. 11B & 11C). For mixing with hydrophobic silica (2% ~ 6%), with the addition of more hydrophobic silica, more complete and faster dissolution of CUR was achieved (Fig. 11B). After mixing with 6% hydrophobic silica, amorphous CUR showed high concentration of CUR (86.60 μg/mL) at 8 h, which exhibited the significant enhancement in dissolution concentration (1.60-fold that of individual amorphous CUR, $p < 0.01$). After adding magnesium stearate to amorphous CUR, a faster dissolution of CUR could be achieved at the initial stage (e.g., 56.98, 64.98 and 71.84 μg/mL after adding 2%, 4% and 6% magnesium stearate at 1 h, respectively) (Fig. 11C). Then amorphous CUR mixing with 2% and 4% magnesium stearate showed similar and higher amount dissolved than that adding 6% magnesium stearate (e.g., 96.45 and 96.87 μg/mL after adding 2% and 4% magnesium stearate, and 86.30 μg/mL after adding 6% magnesium stearate at 8 h). The dissolution concentration of amorphous CUR mixing with 2%, 4% and 6% magnesium stearate showed significant improvements (i.e., 1.78-, 1.78- and 1.59-fold that of individual amorphous CUR, $p < 0.01$). In addition, excipients presence with different temperatures or pHs were investigated on the dissolution of amorphous CUR. As a result, the addition of hydrophobic silica and magnesium stearate could also effectively improve the dissolution rate and dissolution extent of amorphous CUR under other temperature or pH conditions, but hydrophilic silica still had no improvement in the dissolution of amorphous CUR (Fig. S15 and Fig. S16). Therefore, hydrophobic excipients (hydrophobic silica and magnesium stearate) could weaken or eliminate the gelation with significantly improved dissolution of amorphous CUR at different temperatures (25, 37 and 45°C) or pHs (pH 1.2, 4.5 and 6.8).

Visually, the distinct aggregation phenomena of amorphous CUR occurring after addition of hydrophilic silica, hydrophobic silica and magnesium stearate, respectively. Amorphous CUR floated on the surface of the medium and gradually gather to form a mass when contacted with the dissolution medium (Video S1, https://youtu.be/KlNwosP1SNM). Taking the addition of 4% glidants as an example, faster aggregation of amorphous CUR was more easily observed when mixing with hydrophilic silica (Video S2, https://youtu.be/j5HEpsp7pl8), indicating the possibility of more serious gelation. The agglomerated powder formed quickly in presence of 4% hydrophilic silica after 1 min dissolution (Fig. 12a), and a more serious gel mass was formed after dissolution (Fig. 12d), showing the strengthened gelation with the lower dissolution. However, the aggregation of amorphous CUR was obviously weakened and even eliminated after mixing with 4% hydrophobic silica. When the mixed powder was put into the dissolution medium, the powder rapidly dispersed or sunk into the medium without clumping (Fig. 12b & Video S3, https://youtu.be/gkG5yyWDuWY). After dissolution, the surface of the collected sample showed a porous structure (Fig. 12e), which might be due to hydrophobic silica hindering the aggregation of amorphous powder, accelerating the dissolution of more CUR. In addition, the mixed powder of amorphous CUR with 4% magnesium stearate dispersed rapidly without aggregation upon

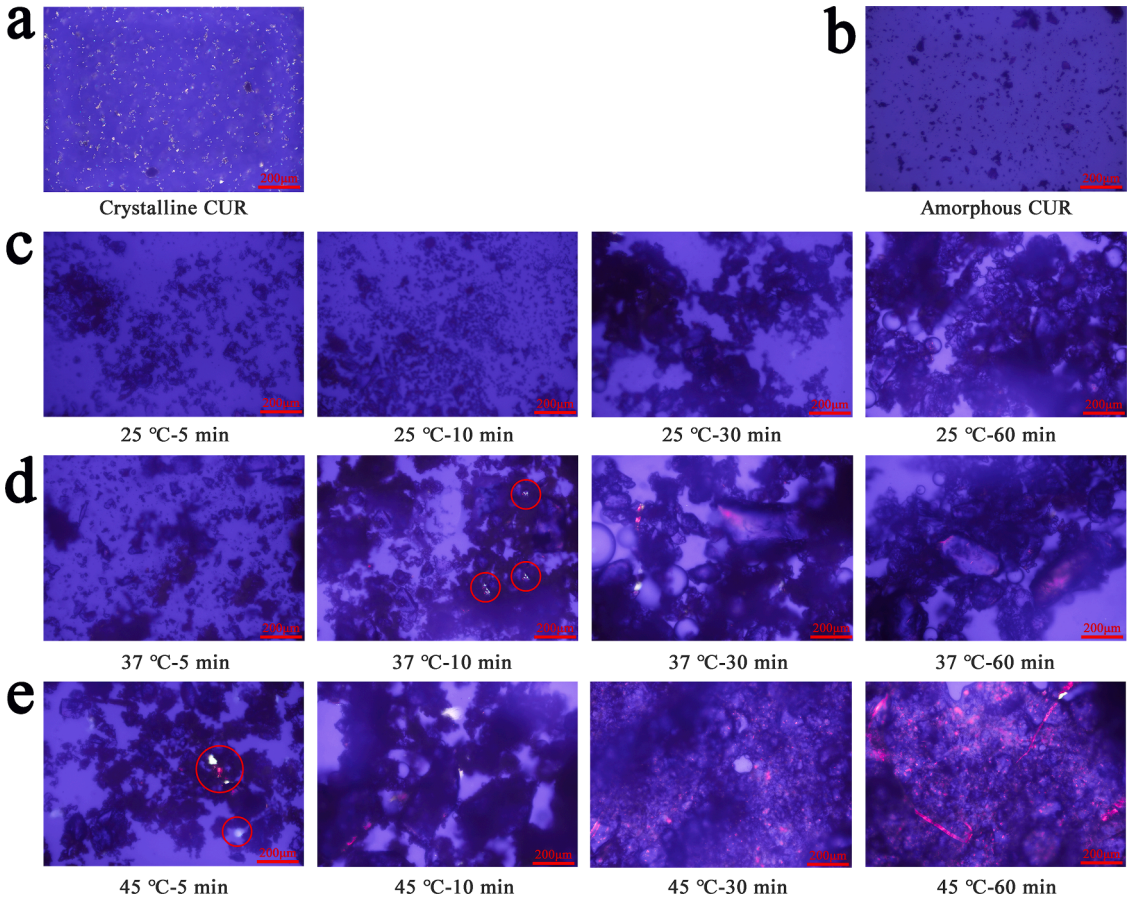

Fig. 10. PLM photographs of samples collected during dissolution of amorphous CUR at 25, 37 and 45°C.

contacting with the medium (Fig. 12c & Video S4, https://youtu.be/Va3K4lKKruA), and no gel formation was observed (Fig. 12f), thus resulting in a significant increase in dissolution. As shown in Video S3 and S4, the particles of amorphous CUR sank rapidly when mixed with hydrophobic silica, while amorphous CUR mixed with magnesium stearate floated on the medium. To investigate the effect of excipient density on amorphous CUR, the bulk density of the powders was determined for hydrophilic silica, hydrophobic silica, magnesium stearate, amorphous CUR and the mixed samples (Table S5). The hydrophilic silica and hydrophobic silica have small bulk density with 0.045 g/mL and 0.041 g/mL, respectively. The lubricant, magnesium stearate, has a bulk density of 0.251 g/mL. When the amorphous CUR was mixed with 4% excipients, the bulk density of the mixed powders did not change significantly compared with that of amorphous CUR. Therefore, the mixed samples floating on the medium or sinking to the bottom of the medium were not necessarily related to the density of the excipients. The added excipients kept the particles separate from one another and prevented the aggregation, resulting in the increase in the surface area and hence the enhanced dissolution rate of amorphous CUR according to Noyes-Whitney equation.

Contact angle is a common technique to investigate the wettability of powders. As seen from Fig. 13, the contact angle of amorphous CUR was 88^{o} (Fig. 13a). By adding hydrophilic silica into amorphous CUR, its contact angle went down to about 71^{o} (Fig. 13b), while the contact angle of amorphous CUR went up to around 127^{o} and 96^{o} after mixing with hydrophobic silica and magnesium stearate (Fig. 13c & d), respectively. Therefore, the addition of hydrophilic silica to the amorphous powder increased its wettability, while mixing with hydrophobic silica and magnesium stearate could reduce the wettability of amorphous CUR. These results indicated that hydrophilic silica promoted water infiltration into the amorphous powder, while hydrophobic silica and magnesium stearate slowed or even hindered water infiltration into the powder interior. To further explore the underlying mechanism, the critical surface tension (γ) of the solid was estimated by the contact angle made by the water on the solid using Zisman approach ($\gamma_{solid} = \gamma_{water} * [\cos\theta + 1]/2$) (Bera et al., 2018; Hill et al., 2016; Owen, 2021). Meanwhile, the interfacial tension between amorphous CUR and excipient was calculated using Antonov approximation ($\gamma_{amorphous\ CUR\ and\ excipient} = ABS(\gamma_{amorphous\ CUR} - \gamma_{excipient})$) (Krichen et al., 2018; Makkonen and Kurkela, 2018). As shown in Table S6, amorphous CUR exhibited the γ of 37.0 mJ/m^2, and hydrophilic silica revealed 28.8 mN/m deviation of amorphous CUR, while hydrophobic silica and magnesium stearate showed small deviations of 2.8 and 7.8 mN/m in comparison to amorphous CUR, respectively, indicating that hydrophobic silica and magnesium stearate had high affinity than hydrophilic silica (Makkonen and Kurkela, 2018). The high affinity between amorphous CUR and excipient effectively provided well physical separation for each other.

Furthermore, fluorescence microscopy was also used to observe the role of the above three excipients in the aggregation of amorphous CUR. Compared with individual amorphous CUR (Video S5, https://youtu.be/sZHEIAMGg-I), when the amorphous powder was mixed with hydrophilic silica, it speeded up the infiltration of water into the powder (Video S6, https://youtu.be/2kybzROmHlA), while when hydrophobic silica and magnesium stearate were added into the powder, a boundary was formed between water and the mixed powder, and water was difficult to penetrate into the powder (Video S7 & S8, https://youtu.be/YYXzyDAOAu4, https://youtu.be/_o8s9bNyX5I). The surface structure of hydrophilic silica is composed of functional groups such as silanol (Si-OH) endowing its hydrophilicity (Fig. S2b). In the mixed powders of amorphous CUR and hydrophilic silica, hydrophilic silica particles played the part of water-absorbing sites, attracting more water clusters

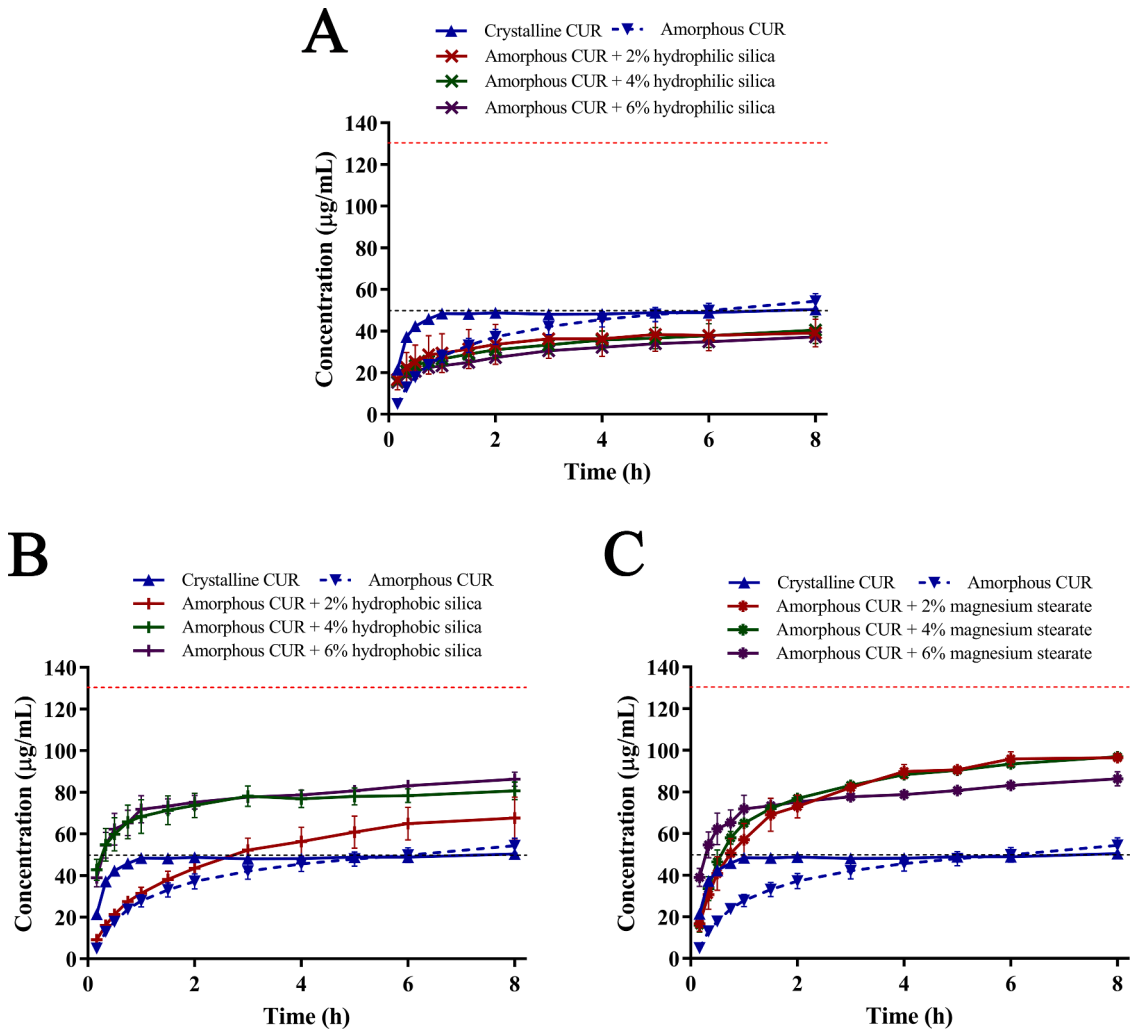

Fig. 11. Dissolution profiles of amorphous CUR in absence and presence of (A) hydrophilic silica, (B) hydrophobic silica and (C) magnesium stearate at weight ratios of 2%, 4% and 6% in pH 6.8 PBS at 37°C (n = 3). For example, 2% means the excipient weight is 2% of the weight of amorphous CUR. The black dotted line represents the equilibrium solubility of crystalline CUR (i.e., 50.32 ± 1.23 μg/mL), and the red dotted line represents the apparent solubility of amorphous CUR (i.e., 130.57 ± 8.29 μg/mL).

into the amorphous powder and hence accelerating gel formation. While for hydrophobic silica (Fig. S2c), it is obtained by an irreversible chemical reaction in combination with dimethylsilyl groups on hydrophilic silica, neither absorbing nor mixing with water (Zhao et al., 2011). Hydrophobic silica adhered to the powder surface of amorphous CUR and prevented the medium from penetrating into the amorphous texture, slowing down or inhibiting the gel formation (Dolatzadeh et al., 2013). When magnesium stearate was mixed with amorphous CUR, it also stuck to the powder surface and effectively promoted the dispersion of amorphous CUR (i.e., aggregation inhibition), eliminating the gelation and hence improving dissolution of amorphous CUR. Therefore, an inference could be drawn that mixing with hydrophilic excipients might accelerate gel formation of amorphous CUR, while hydrophobic excipients could weaken or even eliminate its gelation.

In order to further explore the influence of hydrophilic and hydrophobic excipients on powder aggregation (initial gelation phase), other hydrophilic or hydrophobic excipients were mixed with the amorphous powder to observe dissolution phenomena. When the amorphous powder was evenly mixed with several hydrophilic excipients (glucose, lactose, maltose, sucrose, mannitol and sodium chloride), aggregation time of the amorphous powder ranged from 67 s to 117 s, while after uniform mixing with six hydrophobic excipients (calcium carbonate, calcium hydrophosphate, monocalcium phosphate, calcium citrate, magnesium trisilicate and saccharin), the aggregation time was significantly prolonged, ranging from 215 s to 398 s (Fig. 14). Furthermore, the critical surface tensions of the six hydrophobic excipients were calculated using Zisman approach by their water contact angle (Fig. S17). The six hydrophobic excipients showed small deviations of 7.0 ~ 11.2 mN/m in comparison to amorphous CUR (Table S6), suggesting that the hydrophobic excipients had good affinity with amorphous CUR (Makkonen and Kurkela, 2018). Visually, in comparison with individual amorphous powder, the powder aggregation was more serious after mixing with hydrophilic excipients. The mixed powder adhered more easily to the stirring paddle to form a larger aggregate/cluster. However, the aggregation degree of powder was relatively reduced after mixing with hydrophobic excipients. The mixed powder floated on the surface of the medium and did not gather into larger clumps (Fig. S18). Actually, the particles of hydrophilic excipients served as water-absorbing sites in the mixed powder, absorbing more water clusters into the powder surface and internal site, and hence more serious aggregation. For hydrophobic excipients, they easily adhered to the powder surface, hindered the powder particle contact, and slowed down the penetration of water molecules into the powder. In summary, hydrophilic excipients accelerated the aggregation of amorphous powder, and hence faster gel formation, while hydrophobic excipients could effectively slow or hinder powder aggregation, thus weakening or eliminating gelation.

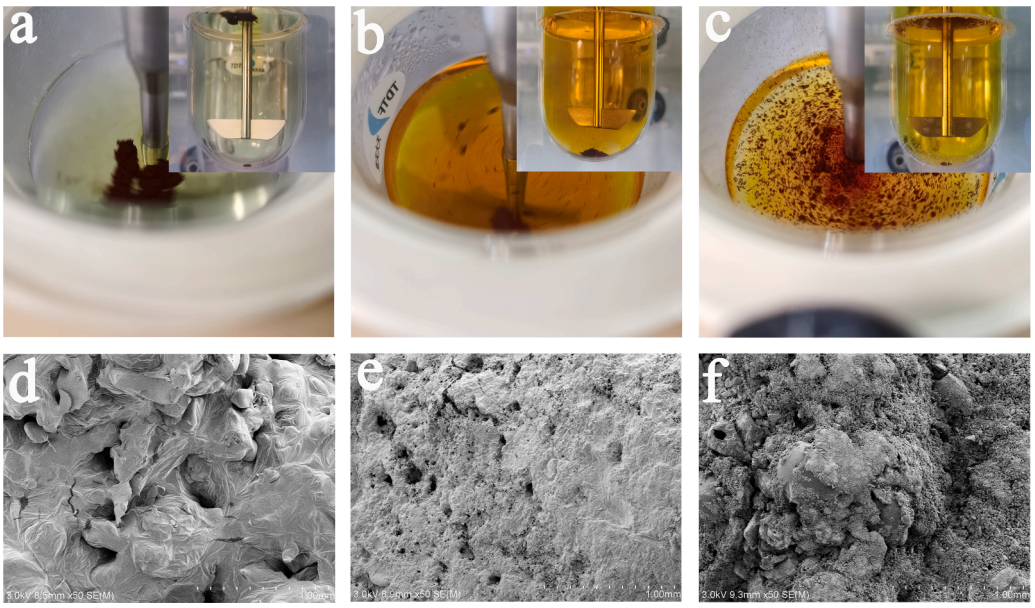

Fig. 12. Photographs of amorphous CUR mixed with (a) 4% hydrophilic silica, (b) 4% hydrophobic silica and (c) 4% magnesium stearate after 1 min dissolution in pH 6.8 PBS at 37°C. SEM images of amorphous CUR mixed with (d) 4% hydrophilic silica, (e) 4% hydrophobic silica and (f) 4% magnesium stearate after dissolution in pH 6.8 PBS at 37°C.

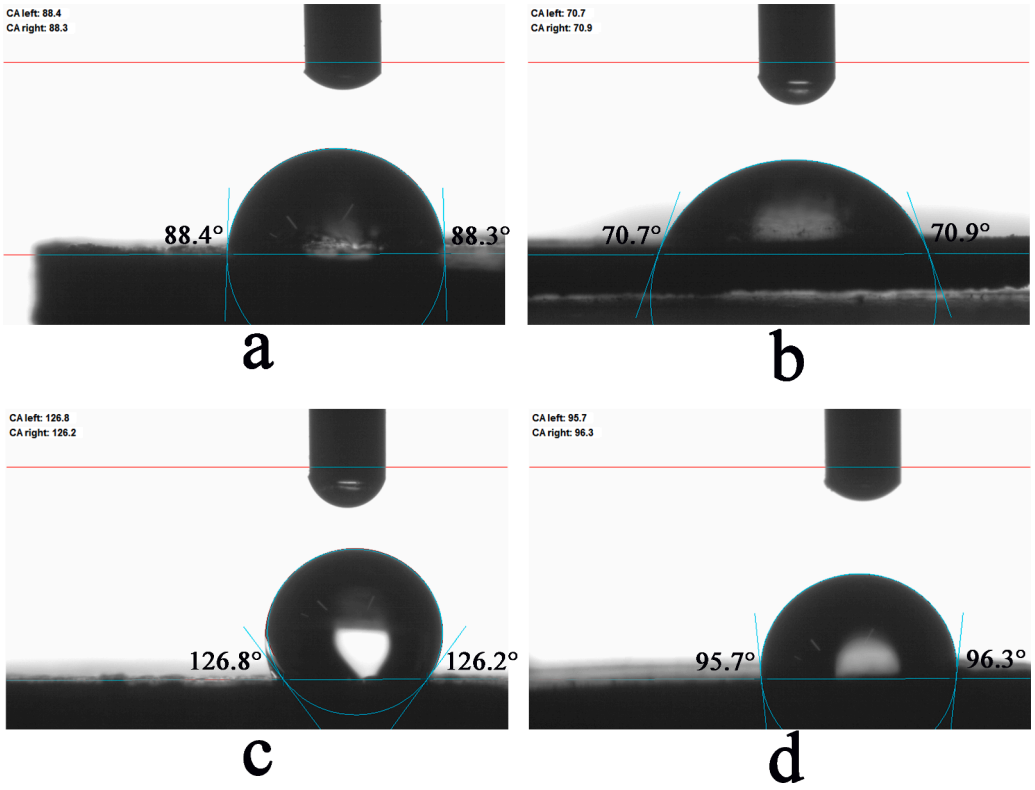

Fig. 13. Contact angle of (a) amorphous CUR and amorphous CUR mixing with (b) 4% hydrophilic silica, (c) 4% hydrophobic silica and (d) 4% magnesium stearate at 10 s.

4. Conclusions

The current study investigated the gel formation of amorphous CUR during dissolution. Multiple characterization (TPA, SEM, DSC, XRPD, FTIR and PLM) results indicated that the gelation process underwent the formation of a porous structure in which water molecules infiltrate, and entered into its supercooled liquid state with high viscosity when contacting aqueous media, accompanied by decreased T_g and recrystallization. Temperature had a more significant effect on gel properties than pH value of dissolution media. Due to gel formation of amorphous CUR during dissolution, it exhibited a decreased dissolution compared with crystalline CUR. Furthermore, mixing with hydrophilic excipients accelerated water entering the interior of amorphous CUR, hence facilitating the gelation, while hydrophobic excipients exhibited

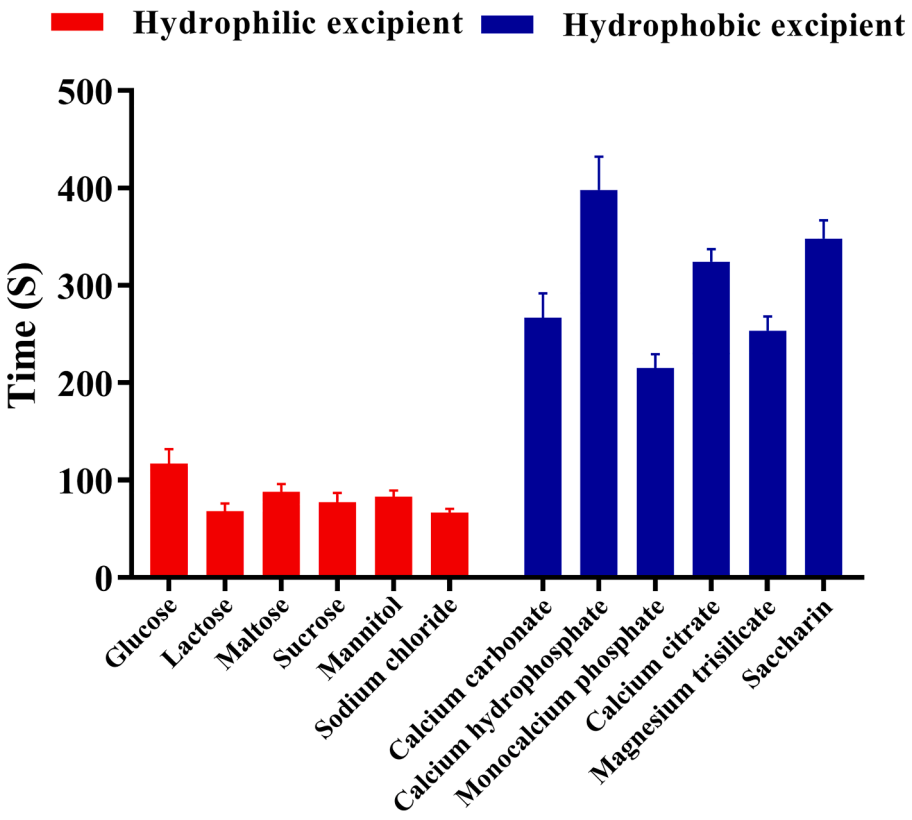

Fig. 14. Aggregation time of amorphous powder after uniform mixing of hydrophilic and hydrophobic excipients in pH 6.8 PBS at 37°C (n = 3).

opposite effect and eliminated the gelation with significantly improved dissolution. In summary, gel-induced aggregation potential of some amorphous materials should be considered in developing robust amorphous drug product of high quality and performance, and deaggregation preferred hydrophobic excipients from a formulation development perspective.

CRediT authorship contribution statement

Jiawei Han: Formal analysis, Writing – original draft, Writing – review & editing. **Luyuan Li:** Investigation, Methodology, Formal analysis. **Zunting Pang:** Conceptualization. **Meiling Su:** Methodology, Supervision. **Xiaoshuang He:** Project administration, Supervision. **Shuai Qian:** Resources, Supervision. **Jianjun Zhang:** Supervision, Project administration. **Yuan Gao:** Funding acquisition, Writing – original draft. **Yuanfeng Wei:** Resources, Writing – review & editing.

Declaration of Competing Interest

The authors declare no conflicts of interest.

Acknowledgements

This research was supported by National Natural Science Foundation of China (82074029, 82104401, 81773675, 81873012), “Double First-Class” University Project (CPU2018GY11, CPU2018GY27), Jiangsu Province Double Innovation Talent Program (2015), Postgraduate Research & Practice Innovation Program of Jiangsu Province (KYCX20_0675), Natural Science Foundation of Jiangsu Province (SBK2020042291), China Postdoctoral Science Foundation Funded Project (2020M671665).

Supplementary materials

Supplementary material associated with this article can be found, in the online version, at doi:10.1016/j.ejps.2021.106083.

References

Ahmed, S., Corvis, Y., Gahoual, R., Euan, A., Lai-Kuen, R., Couillaud, B.M., Seguin, J., Alhareth, K., Mignet, N., 2019. Conception of nanosized hybrid liposome/poloxamer particles to thicken the interior core of liposomes and delay hydrophilic drug delivery. Int. J. Pharm. 567, 118488.
Ambike, A.A., Mahadik, K.R., Paradkar, A., 2005. Spray-dried amorphous solid dispersions of simvastatin, a low tg drug: in vitro and in vivo evaluations. Pharm. Res. 22, 990–998.
Baral, A., Basak, S., Basu, K., Dehsorkhi, A., Hamley, I.W., Banerjee, A., 2015. Time-dependent gel to gel transformation of a peptide based supramolecular gelator. Soft matter 11, 4944–4951.
Bera, B., Carrier, O., Backus, E.H.G., Bonn, M., Shahidzadeh, N., Bonn, D., 2018. Counteracting interfacial energetics for wetting of hydrophobic surfaces in the presence of surfactants. Langmuir 34, 12344–12349.
Bhasker-Ranganath, S., Rahman, M.S., Zhao, C., Calaza, F., Wu, Z., Xu, Y., 2021. Elucidating the mechanism of ambient-temperature aldol condensation of acetaldehyde on ceria. ACS Catal. 11, 8621–8634.
Brouwers, J., Brewster, M.E., Augustijns, P., 2009. Supersaturating drug delivery systems: the answer to solubility-limited oral bioavailability? J. Pharm. Sci. 98, 2549–2572.
Chen, Z., Xia, Y., Liao, S., Huang, Y., Li, Y., He, Y., Tong, Z., Li, B., 2014. Thermal degradation kinetics study of curcumin with nonlinear methods. Food Chem. 155, 81–86.
Cok, M., Viola, M., Vecchies, F., Sacco, P., Furlani, F., Marsich, E., Donati, I., 2020. N-isopropyl chitosan. A pH- and thermo-responsive polysaccharide for gel formation. Carbohydr. Polym. 230, 115641.
Dolatzadeh, F., Jalili, M.M., Moradian, S., 2013. Influence of various loadings of hydrophilic or hydrophobic silica nanoparticles on water uptake and porosity of a polyurethane coating. Mater. Corros. 64, 609–618.
Edueng, K., Mahlin, D., Larsson, P., Bergstrom, C.A.S., 2017. Mechanism-based selection of stabilization strategy for amorphous formulations: Insights into crystallization pathways. J. Control. Release 256, 193–202.
Estroff, L.A., Hamilton, A.D., 2004. Water gelation by small organic molecules. Chem. Rev. 104, 1201–1218.
Flory, P.J., 1974. Introductory lecture. Faraday Discuss. Chem. Soc. 57, 7–18.

Forster, S.P., Lebo, D.B., 2021. Continuous melt granulation for taste-masking of ibuprofen. Pharmaceutics 13, 863.
Franca, M.T., Marcos, T.M., Pereira, R.N., Stulzer, H.K., 2020. Could the small molecules such as amino acids improve aqueous solubility and stabilize amorphous systems containing Griseofulvin? Eur. J. Pharm. Sci. 143, 105178.
Fujiki, S., Iwao, Y., Kobayashi, M., Miyagishima, A., Itai, S., 2011. Stabilization mechanism of clarithromycin tablets under gastric pH conditions. Chem. Pharm. Bull. 59, 553–558.
Fung, M., Be Rzins, K.R., Suryanarayanan, R., 2018. Physical stability and dissolution behavior of ketoconazole-organic acid coamorphous systems. Mol. Pharm. 15, 1862–1869.
George, M., Weiss, R.G., 2006. Molecular organogels. Soft matter comprised of low-molecular-mass organic gelators and organic liquids. Acc. Chem. Res. 39, 489–497.
Han, J., Wei, Y., Lu, Y., Wang, R., Zhang, J., Gao, Y., Qian, S., 2020. Co-amorphous systems for the delivery of poorly water-soluble drugs: Recent advances and an update. Expert Opin. Drug Deliv. 17, 1411–1435.
Hayakawa, E., Furuya, K., Kuroda, T., Moriyama, M., Kondo, A., 1990. Studies on the dissolution behavior of doxorubicin hydrochloride freeze-dried product. Chem. Pharm. Bull. 38, 3434–3439.
Heng, W., Wei, Y., Xue, Y., Cheng, H., Zhang, L., Zhang, J., Gao, Y., Qian, S., 2019a. Gel formation induced slow dissolution of amorphous indomethacin. Pharm. Res. 36, 159.
Heng, W., Wei, Y., Zhou, S., Ma, D., Gao, Y., Zhang, J., Qian, S., 2019b. Effects of temperature and ionic strength of dissolution medium on the gelation of amorphous lurasidone hydrochloride. Pharm. Res. 36, 72.
Hill, M.J., Cheah, C., Sarkar, D., 2016. Interfacial energetics approach for analysis of endothelial cell and segmental polyurethane interactions. Colloids Surf B. Biointerfaces 144, 46–56.
Hou, G., Wang, Z., Ma, H., Ji, Y., Yu, L., Xu, J., Chen, K., 2019. High-temperature stable plasmonic and cavity resonances in metal nanoparticle-decorated silicon nanopillars for strong broadband absorption in photothermal applications. Nanoscale 11, 14777–14784.
Huang, M., Kennedy, J.F., Li, B., Xu, X., Xie, B.J., 2007. Characters of rice starch gel modified by gellan, carrageenan, and glucomannan: A texture profile analysis study. Carbohydr. Polym. 69, 411–418.
Huang, R., Han, J., Wang, R., Zhao, X., Qiao, H., Chen, L., Li, W., Di, L., Zhang, W., Li, J., 2019. Surfactant-free solid dispersion of BCS class IV drug in an amorphous chitosan oligosaccharide matrix for concomitant dissolution in vitro - permeability increase. Eur. J. Pharm. Sci. 130, 147–155.
Karmwar, P., Graeser, K., Gordon, K.C., Strachan, C.J., Rades, T., 2012. Effect of different preparation methods on the dissolution behaviour of amorphous indomethacin. Eur. J. Pharm. Biopharm. 80, 459–464.
Kasten, G., Lobmann, K., Grohganz, H., Rades, T., 2019. Co-former selection for co-amorphous drug-amino acid formulations. Int. J. Pharm. 557, 366–373.
Kaur, R., Khullar, P., Mahal, A., Gupta, A., Singh, N., Ahluwalia, G.K., Bakshi, M.S., 2018. Keto-enol tautomerism of temperature and pH sensitive hydrated curcumin nanoparticles: their role as nanoreactors and compatibility with blood cells. J. Agric. Food Chem. 66, 11974–11980.
Kim, J.S., Kim, M.S., Park, H.J., Jin, S.J., Lee, S., Hwang, S.J., 2008. Physicochemical properties and oral bioavailability of amorphous atorvastatin hemi-calcium using spray-drying and SAS process. Int. J. Pharm. 359, 211–219.
Kim, M., Lee, H., Kim, M., Park, Y.C., 2021. Coloration and chromatic sensing behavior of electrospun cellulose fibers with curcumin. Nanomaterials 11, 222.
Kim, M.J., Shin, S.H., Kim, Y.J., Cheong, M., Lee, J.S., Kim, H.S., 2013. Role of alkyl group in the aromatic extraction using pyridinium-based ionic liquids. J. Phys. Chem. B 117, 14827–14834.
Krichen, F., Sila, A., Caron, J., Kobbi, S., Nedjar, N., Miled, N., Blecker, C., Besbes, S., Bougatef, A., 2018. Identification and molecular docking of novel ACE inhibitory peptides from protein hydrolysates of shrimp waste. Eng. Life Sci. 18, 682–691.
Kumar, R., Lee, Y.K., Jho, Y.S., 2020. Martini coarse-grained model of hyaluronic acid for the structural change of its gel in the presence of monovalent and divalent salts. Int. J. Mol. Sci. 21, 4602.
Makkonen, L., Kurkela, J., 2018. Another look at the interfacial interaction parameter. J. Colloid Interface Sci. 529, 243–246.
Matlinska, M.A., Wasylishen, R.E., Bernard, G.M., Terskikh, V.V., Brinkmann, A., Michaelis, V.K., 2018. Capturing elusive polymorphs of curcumin: A structural characterization and computational study. Cryst. Growth Des. 18, 5556–5563.
Meulenaar, J., Beijnen, J.H., Schellens, J.H., Nuijen, B., 2013. Slow dissolution behaviour of amorphous capecitabine. Int. J. Pharm. 441, 213–217.
Owen, M.J., 2021. Silicone surface fundamentals. Macromol. Rapid Commun. 42, e2000360.
Paisana, M.C., Lino, P.R., Nunes, P.D., Pinto, J.F., Henriques, J., Paiva, A.M., 2021. Laser diffraction as a powerful tool for amorphous solid dispersion screening and dissolution understanding. Eur. J. Pharm. Sci. 163, 105853.
Piovesan, E., Campana, P.T., Arantes, T.M., Ribeiro, D.A., Marletta, A., Cristovan, F.H., 2020. Energy transfer mechanisms in pH-tuned aggregates of curcumin. Spectrochim. Acta A Mol. Biomol. Spectrosc. 225, 117521.
Pires, P.C., Fazendeiro, A.C., Rodrigues, M., Alves, G., Santos, A.O., 2021. Nose-to-brain delivery of phenytoin and its hydrophilic prodrug fosphenytoin combined in a microemulsion - formulation development and in vivo pharmacokinetics. Eur. J. Pharm. Sci. 164, 105918.
Qian, S., Wang, S., Li, Z., Wang, X., Ma, D., Liang, S., Gao, Y., Zhang, J., Wei, Y., 2017. Charge-assisted bond N(+)H mediates the gelation of amorphous lurasidone hydrochloride during dissolution. Int. J. Pharm. 518, 335–341.
Qian, S.A., Heng, W.L., Wei, Y.F., Zhang, J.J., Gao, Y., 2015. Coamorphous lurasidone hydrochloride-saccharin with charge-assisted hydrogen bonding interaction shows improved physical stability and enhanced dissolution with pH-independent solubility behavior. Cryst. Growth Des. 15, 2920–2928.
Ray, P., Gray, J.L., Badding, J.V., Lueking, A.D., 2016. High-pressure reactivity of triptycene probed by Raman spectroscopy. J. Phys. Chem. B 120, 11035–11042.
Sahoo, A., Kumar, N.S.K., Suryanarayanan, R., 2019. Crosslinking: an avenue to develop stable amorphous solid dispersion with high drug loading and tailored physical stability. J. Control. Release 311-312, 212–224.
Sanphui, P., Bolla, G., 2018. Curcumin, a biological wonder molecule: A crystal engineering point of view. Cryst. Growth Des. 18, 5690–5711.
Sanphui, P., Goud, N.R., Khandavilli, U.B., Bhanoth, S., Nangia, A., 2011. New polymorphs of curcumin. Chem. Commun. 47, 5013–5015.
Satapute, P., Jogaiah, S., 2021. A biogenic microbial biosurfactin that degrades difenoconazole fungicide with potential antimicrobial and oil displacement properties. Chemosphere 286, 131694.
Shi, X., Song, S., Ding, Z., Fan, B., Huang, W., Xu, T., 2019. Improving the solubility, dissolution, and bioavailability of ibrutinib by preparing it in a coamorphous state with saccharin. J. Pharm. Sci. 108, 3020–3028.
Shi, X., Zhou, X., Shen, S., Chen, Q., Song, S., Gu, C., Wang, C., 2021. Improved in vitro and in vivo properties of telmisartan in the co-amorphous system with hydrochlorothiazide: a potential drug-drug interaction mechanism prediction. Eur. J. Pharm. Sci. 161, 105773.
Tavares, L., Santos, L., Noreña, C.P.Z., 2021. Microencapsulation of organosulfur compounds from garlic oil using β-cyclodextrin and complex of soy protein isolate and chitosan as wall materials: a comparative study. Powder Technol 390, 103–111.
Trubitsyn, G., Nga Nguyen, V., Di Tommaso, C., Borchard, G., Gurny, R., Moller, M., 2019. Impact of covalently nile red and covalently rhodamine labeled fluorescent polymer micelles for the improved imaging of the respective drug delivery system. Eur. J. Pharm. Biopharm. 142, 480–487.
Trucillo, P., Campardelli, R., Reverchon, E., 2018. Production of liposomes loaded with antioxidants using a supercritical CO_2 assisted process. Powder Technol 323, 155–162.
Wang, L., Yu, C., Chang, T., Zhang, M., Song, S., Xiong, C., Su, P., Xiang, W., 2020. In situ repair abilities of human umbilical cord-derived mesenchymal stem cells and autocrosslinked hyaluronic acid gel complex in rhesus monkeys with intrauterine adhesion. Sci. Adv. 6, eaba6357.
Wang, R., Han, J., Jiang, A., Huang, R., Fu, T., Wang, L., Zheng, Q., Li, W., Li, J., 2019. Involvement of metabolism-permeability in enhancing the oral bioavailability of curcumin in excipient-free solid dispersions co-formed with piperine. Int. J. Pharm. 561, 9–18.
Wang, Z., Mu, W., Li, P., Liu, G., Yang, J., 2021. Anti-inflammatory activity of ortho-trifluoromethoxy-substituted 4-piperidione-containing mono-carbonyl curcumin derivatives in vitro and in vivo. Eur. J. Pharm. Sci. 160, 105756.
Wei, Y., Zhou, S., Hao, T., Zhang, J., Gao, Y., Qian, S., 2019. Further enhanced dissolution and oral bioavailability of docetaxel by coamorphization with a natural P-gp inhibitor myricetin. Eur. J. Pharm. Sci. 129, 21–30.
Wimalasiri, V.W., Dunuweera, S.P., Dunuweera, A.N., Rajapakse, R.M.G., 2021. Noyes-whitney dissolution model-based ph-sensitive slow release of paclitaxel (taxol) from human hair-derived keratin microparticle carriers. Biomed. Res. Int. 2021, 6657482.
Wu, W., Lobmann, K., Rades, T., Grohganz, H., 2018a. On the role of salt formation and structural similarity of co-formers in co-amorphous drug delivery systems. Int. J. Pharm. 535, 86–94.
Wu, W., Lobmann, K., Schnitzkewitz, J., Knuhtsen, A., Pedersen, D.S., Grohganz, H., Rades, T., 2018b. Aspartame as a co-former in co-amorphous systems. Int. J. Pharm. 549, 380–387.
Xie, Y., Yao, Y., 2020. Preparation and characterization of a solid dispersion containing curcumin and octenylsuccinate hydroxypropyl phytoglycogen for improved curcumin solubility. Eur. J. Pharm. Sci. 153, 105462.
Yao, J., Zhou, Y., Chen, X., Ma, F., Li, P., Chen, C., 2018. Effect of sodium alginate with three molecular weight forms on the water holding capacity of chicken breast myosin gel. Food Chem. 239, 1134–1142.
Zhao, Y., Li, J., Hu, J., Shu, L., Shi, X., 2011. Fabrication of super-hydrophobic surfaces with long-term stability. J. Disper. Sci. Technol. 32, 969–974.
Zhu, M., Wang, J.Q., Perepezko, J.H., Yu, L., 2015. Possible existence of two amorphous phases of D-mannitol related by a first-order transition. J. Chem. Phys. 142, 244504.